The 5th European sCO2 Conference for Energy Systems
March 14-16, 2023, Prague, Czech Republic

2023-sCO2.eu-136

DESIGN AND TESTING OF A SUPERCRITICAL CO_2 COMPANDER FOR 2 MW OUTPUT POWER

Markus Sauerborn*
Atlas Copco Gas and Process
Cologne, Germany
Email: markus.sauerborn@atlascopco.com

Ulrich Schmitz
Atlas Copco Gas and Process
Cologne, Germany
Email: ulrich.schmitz@atlascopco.com

Dr. Jürgen Bohn
Atlas Copco Gas and Process
Cologne, Germany
Email:
juergen.bohn@atlascopco.com

Dr. Martin Enneking
Atlas Copco Gas and Process
Cologne, Germany
Email:
martin.enneking@atlascopco.com

Jens Brenner
Atlas Copco Gas and Process
Cologne, Germany
Email:
jens.brenner@atlascopco.com

ABSTRACT

Around the globe, there has been a growing interest in using sCO_2 power cycles to recover waste heat from various heat sources. This paper will focus on the case of a supercritical CO_2 compander designed, built, tested, and supplied by the authors' company.

The compander is applied in a Brayton cycle to recover waste heat from a gas engine providing the output power to a generator connected to a gear box via a coupling. To design the heat-recovery cycle with the highest possible efficiency, a low-operation temperature at the compressor inlet was required. At the given pressure, this leads to a subcooled fluid.

With support from the client and additional internal studies, it was confirmed that this suction condition at the compressor inlet will lead to the lowest power consumption on the compression side. This, in turn, results in the highest cycle efficiency, in addition to a small machinery footprint. Therefore, the solution fits into marine applications or other projects which face space constraints.

During the compression process, a phase change of the CO_2 from the subcooled to the supercritical state occurs with a low temperature and density change. CFD simulations of the compression process were performed in advance, considering the real fluid behavior near the critical point.

This paper presents the test results and a comparison with the CFD analysis.

INTRODUCTION

Starting back in 1984, Atlas Copco Gas and Process began its involvement in many projects and activities that have aimed at carbon-footprint reduction with its supply of centrifugal compressors and expanders. Since then, the company has delivered compressors for CO_2 compression that rises from 1 bar in eight stages of compression to 202 bar.

Building on these technological advancements, another step was to develop a machine design that could be applied in an sCO_2 Brayton cycle for waste heat recovery applications. Since these demands are driven by the market, the process and the associated design conditions for the compressor and the turbine are typically defined by our client.

For the case presented in this paper, among the various investigated sCO_2 cycle configurations for power generation applications [1], due to the moderate turbine inlet temperature of below 300 °C, a simple recuperated Brayton cycle was selected for the demo plant [2, 3]. Besides simplicity, this configuration allows for the implementation of a single-stage compressor – and a single-stage turbine stage combined on the same gearbox (compander) as intended for highest compactness.

* corresponding author(s)

DOI: 10.17185/duepublico/77319

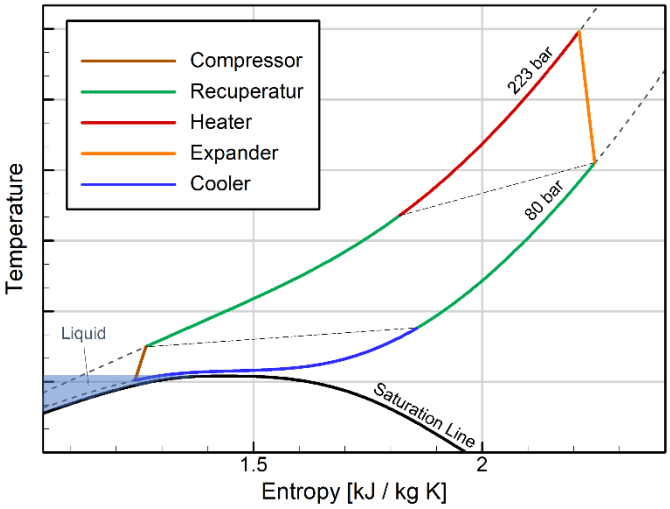

Figure 1: Ts-diagram of sCO_2 power cycle

As shown in Figure 1, the compression inlet conditions are specified with 80 bar and 28 °C, i.e. in the liquid phase of the CO_2, which is a novelty in compression technology. Supported by our client and with further internal studies, it was confirmed that this point will lead to the lowest power consumption on the compression side, resulting in the highest cycle efficiency combined with a small footprint of machinery, which fits nicely into marine applications or projects having space constrains (see Table 1).

length (up to bullgear shaft end)	mm	1442
width	mm	2160
height	mm	1410

Table 1: overall dimensions of compander

Following the R&D study and subsequent hardware orders, Atlas Copco Gas and Process supplied the project's sCO_2 compander for the sCO_2 power cycle, which recovered waste heat from the gas-engine driver.

WASTE-HEAT RECOVERY CYCLE AND MACHINE DESIGN

Figure 2 shows the machine layout principle of the compander and its implementation in the sCO_2 cycle. This is an integrally geared design in which the single-stage centrifugal-type compressor and the single-stage turbine stage are running back-to-back on the same pinion, and connected to the generator via bull gear and coupling on a single gearbox.

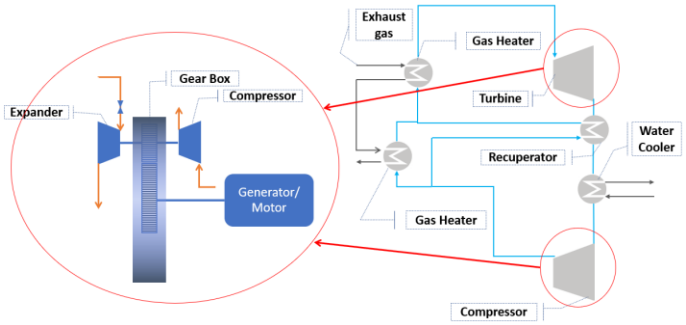

Figure 2: Compander layout principle & process flow diagram

The client intended to install the compander on its test site, which had a gas engine available as the heat source. The sCO_2 Brayton cycle was designed to recover 2 MW of the exhaust heat of the engine as net output power.

The thermal efficiency of the Brayton cycle is defined as the ratio of net output power (= turbine power minus compressor power) divided by the input heat flow:

$$\eta_{th} = \frac{|P_T| - |P_C|}{|\dot{Q}_{heat}|} \quad (1)$$

The Gibbs equation follows from the 1st and the 2nd laws of thermodynamics of a reversible process:

$$dh = Tds + \frac{dp}{\rho} \quad (2)$$

It can be concluded, therefore, that for achieving the same pressure increase *dp* at the same losses *Tds*, the lowest compressor work input *dh* is required, when the average density is high [4].

Near the critical pressure, CO_2 shows a strong dependency on the density when the temperature is varied only slightly around the critical temperature. For example, at 80 bar the density jumps from 613.7 kg/m³ to 736.5 kg/m³ when the temperature is decreased from 33 °C to 28 °C (see Figure 3).

DOI: 10.17185/duepublico/77319

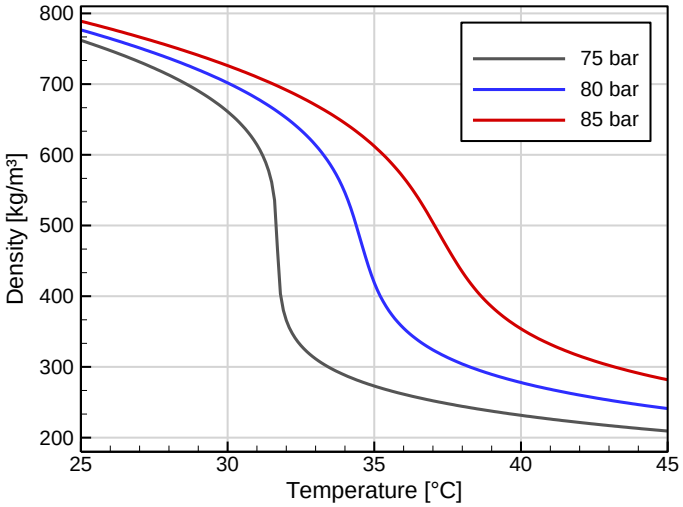

Figure 3: Density of CO_2 near the critical point (NIST REFPROP)

Table 2 shows the relative increase of compressor power required for the compression from 80 to 223 bar (at constant efficiency), when the inlet temperature is varied between 28 and 33°C.

$T_{C,inlet}$ [°C]	relative power $P_C/P_C@28°C$
28	1.000
31	1.060
33	1.136

Table 2: Relative power vs compressor inlet temperature

Equation 1 (see above, page 2) means that for highest-thermal cycle efficiency, the compressor inlet conditions are found in the liquid phase of CO_2, just left to the critical point.

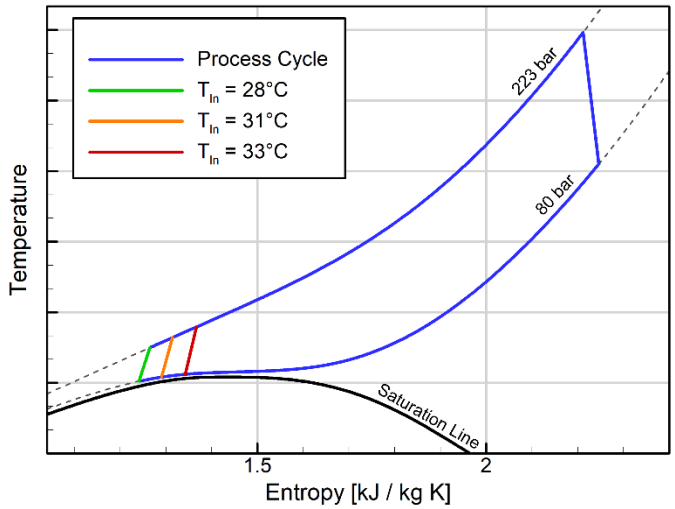

Figure 4: Ts-diagram simple Brayton Cycle for variation of the compressor inlet temperature

Figure 4 shows the shift of the Brayton cycle in the Ts-diagram for the variation of the compressor inlet temperature.
To avoid falling into the two-phase region, some margin to the saturation line must be kept, as shown in the zoomed area of the Ts-diagram in Figure 5.

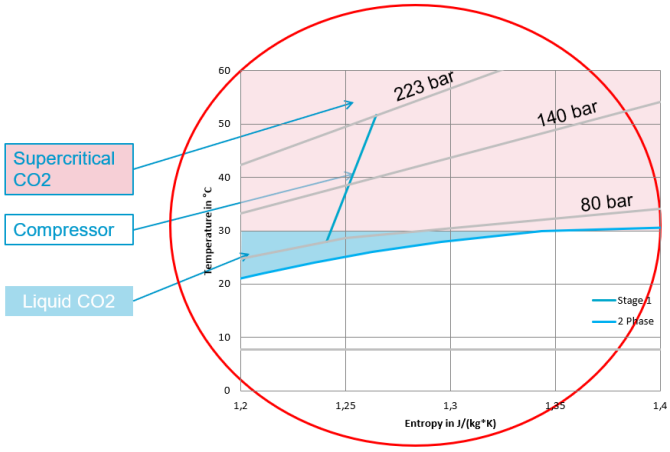

Figure 5: Ts-diagram: zoomed area compressor operating conditions

Finally, the compressor inlet pressure was set to 80 bar and the inlet temperature to 28 °C. At these inlet conditions and with an outlet pressure of 223 bar, the compression process takes place from the liquid to supercritical state, which is an innovation because such compressors are not yet available on the commercial market.

The associated challenges for the aero and mechanical design of the machine were accepted, and it was agreed with the client to carry out theoretical and experimental investigations on the compression process in parallel to delivering the compander unit.

CFD SIMULATION

A CFD (computational fluid dynamics) analysis of the compressor stage was performed using ANSYS CFX software [5]. The CFD model comprises a single-blade channel of the shrouded impeller, including the inducer part, and the impeller labyrinth seal, followed by the full 360° vaneless diffuser and the volute casing (see Figure 6). Frozen rotor interfaces connect the inducer with the impeller and labyrinth seal. The outlet of the impeller is connected via a mixing plane interface to the full 360° diffuser domain. A General Grid Interface (GGI) is used to connect the diffuser and volute.

Inlet boundary conditions are total pressure and total temperature derived from test conditions, and the wall functions approach with $y^+ \approx 50$ is applied to model the wall boundary layers. $k\omega$-SST was selected as turbulence model.

DOI: 10.17185/duepublico/77319

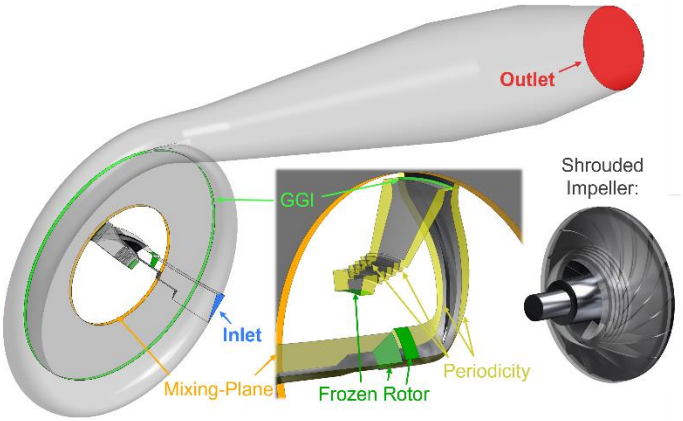

Figure 6: Domain for CFD analysis

The total grid size is 12.7 mio nodes, as shown in Table 3, and the main aerodynamic design parameters of the compressor stage are shown in Table 4.

Inducer (1 passage)	0.5 mio
Impeller (1 passage)	4.3 mio
Labyrinth sealing area (1 passage)	1.1 mio
Diffuser (360 °)	5.0 mio
Volute	1.8 mio
Total	**12.7 mio**

Table 3: Grid size of the CFD model

Impeller type		centrifugal, shrouded
Shaft sealing		dry face seal
Impeller outer diameter	mm	104
Speed	rpm	38000
Mass flow	kg/h	174600
Inlet pressure	bar	80
Inlet temperature	°C	28
Outlet pressure	bar	223

Table 4: Aerodynamic design parameters of the compressor

Because the compressor inlet operates at a subcooled condition near the saturation line and at outlet at a supercritical condition, a real gas property approach is mandatory for the CFD setup. Therefore, the NIST REFPROP real gas property database was incorporated into the CFD model, and the fluid is modelled as a homogeneous mixture of (subcooled) liquid and vapor.

In the following, the mass fraction of vapor and the density inside the impeller channel, and the labyrinth seal are shown at design point operation (see Table 4).

As expected, a sudden phase change of the CO_2 from the liquid to the supercritical phase in the first third of the blade chord is observed, while the density increases smoothly from impeller inlet to outlet (see Figure 7, right-hand side).

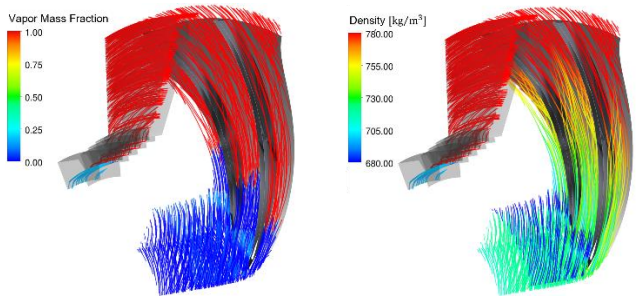

Figure 7: Vapor mass fraction and density of impeller and labyrinth seal flow

The smooth density increase results in a smooth blade loading distribution along the suction and pressure side (see Figure 8).

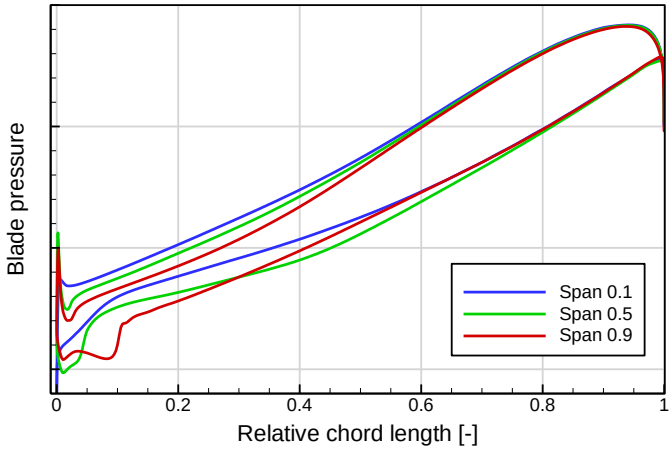

Figure 8: Blade loading at span 0.1, 0.5 and 0.9

TEST SET-UP AND SAFETY ISSUES

To demonstrate the compression process and machine integrity as well as to validate the CFD results, a second identical test unit was built in addition to the client machine for in-house performance testing with CO_2 at original operating conditions.

Since the investigations were focused on the compressor only, the expander was not tested. This means the actual CO_2 test cycle consisted of the compressor stage, a recycle valve, and a cooler only (see Figure 9).

DOI: 10.17185/duepublico/77319

1. Compressor stage
2. Inlet pipe
3. Discharge pipe
4. Temperature & pressure tappping for performance measurement

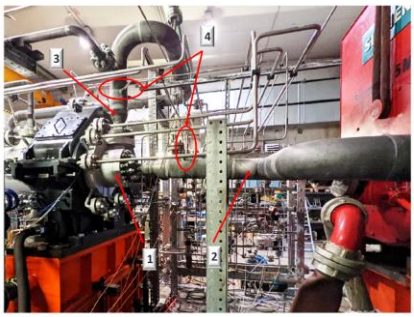

Figure 9: sCO_2 test unit

On the other side of the common pinion shaft a dummy disk was mounted instead of the expander impeller to serve as an axial thrust compensation cylinder for the compressor impeller. The expander housing was pressurized with helium at an appropriate pressure to balance the axial force. Although no blading existed on the dummy expander disk and the viscosity of helium was low, a significant amount of heat was generated in the expander housing due to disk friction. Therefore, an additional cooling system for the expander housing using liquid nitrogen had to be installed (see Figure 10).

1. Core Unit
2. Expander
3. Compressor loop (filled with CO2)
4. Orifice (for flow measurement)
5. Throttle valve
6. Oil supply system
7. Cooling system for expander casing
8. Seal gas panel

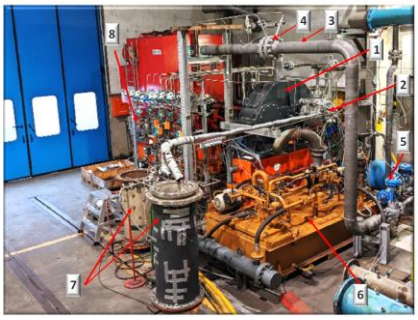

Figure 10: sCO_2 test loop with periphery

As well as the installation of a safety relief valve, in order to ensure safe operation an emergency shut-down scenario was performed using the dynamic process simulation software UniSim Design [6] for determination and evaluation of the settle-out pressure and the expected state of the CO_2 after standstill or machine trip (see Figure 11).

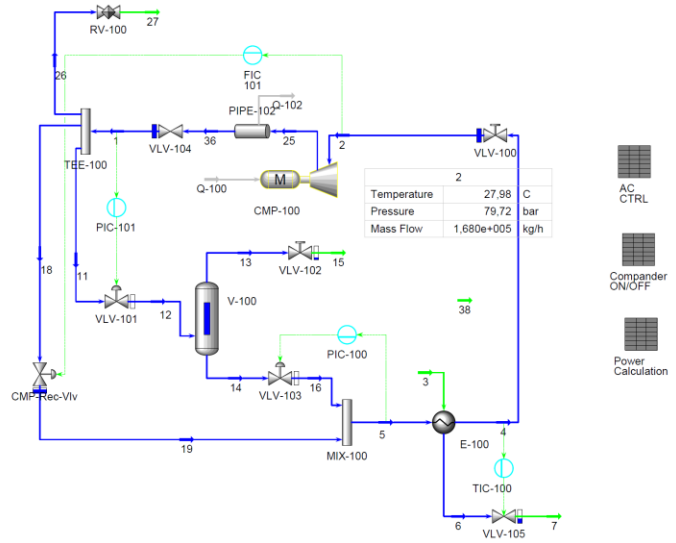

Figure 11: Dynamic simulation model of the test set-up.

The solver calculates the heat and mass balance using pressure flow relations of the components as further input. NIST REFPROP was selected as gas property package. For calculating the machine trip scenario, the volumes of all components in the loop, such as piping, heat exchangers, and so on must be specified. Further input variables are the compressor performance curves, the Cv values, and the rotational inertia of the complete drive train.

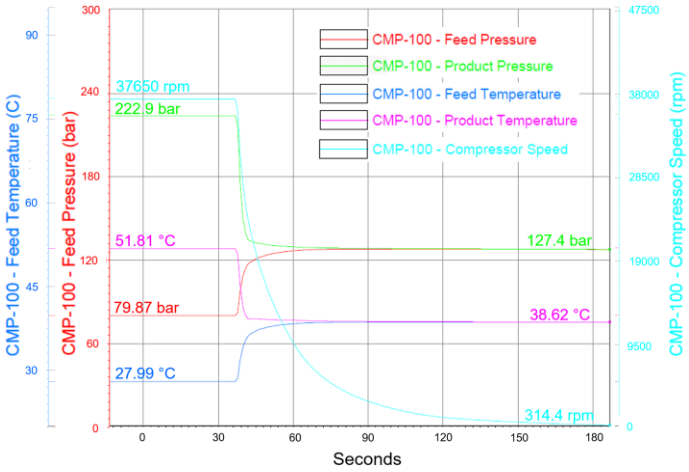

Figure 12: Pressure and temperature trends at compressor inlet and outlet after a machine trip.

Figure 12 shows the pressure and temperature trends at compressor inlet and outlet after a machine trip. As settle out conditions, a pressure of 127 bar and a temperature of 39 °C are calculated. This means, after a machine trip, the CO2 remains in the supercritical phase and the possible maximum pressure in the loop is safely below the mechanical-design pressure of the components.

DOI: 10.17185/duepublico/77319

Due to the excessive pressure of the CO_2 in the loop of up to 242 bar, a HAZOP (hazard and operability) analysis was also carried out with test-service provider TÜV Rheinland. As a residual risk, the failure of the dry face shaft-sealing system was identified. At nominal operating conditions, a small amount of leakage gas passed through the contact-free shaft sealing, which is a system of labyrinths, carbon rings, and a dry face seal as the main sealing element (see Figure 13).

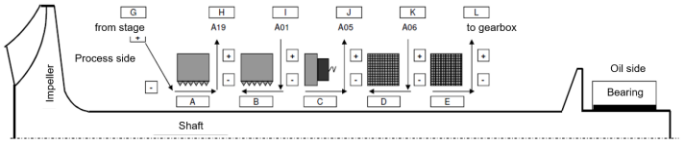

Figure 13: Shaft sealing system of the sCO2 compressor stage

Figure 14 shows the associated seal-gas panel connected to the compressor stage.

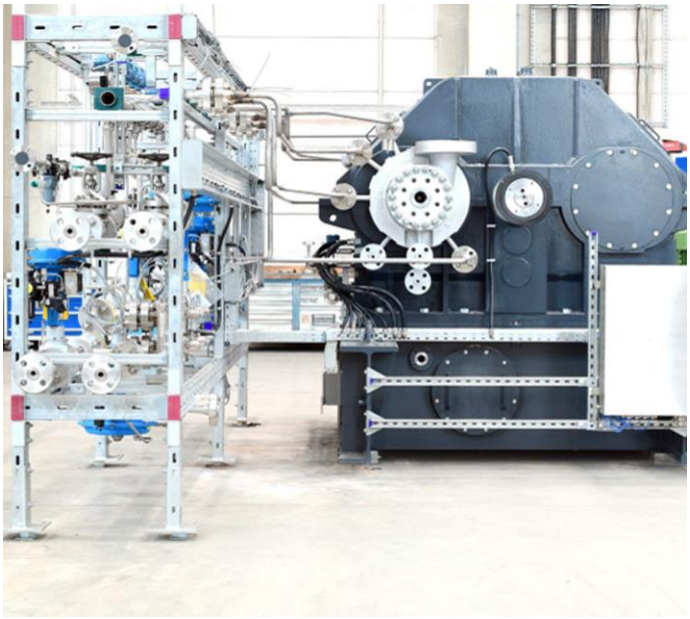

Figure 14: sCO_2 compressor & seal-gas panel

In case of a failure of the dry gas seal, the labyrinths and carbon rings would also be damaged due to increased shaft vibration, while an excessive amount of process gas would flow via the gearbox into the oil tank.

The oil tank is a non-pressurized reservoir with a venting line outside to the atmosphere. Due to the limited capacity of venting gas to the atmosphere, there might be a potential risk of blowing up the oil tank. Therefore, another simulation was carried out in which the damaged seal parts were simulated as throttling elements. Figure 15 shows the Ts-diagram of the expansion process, starting from the impeller outlet pressure of 169 bar in a supercritical state to atmospheric pressure in the two-phase region.

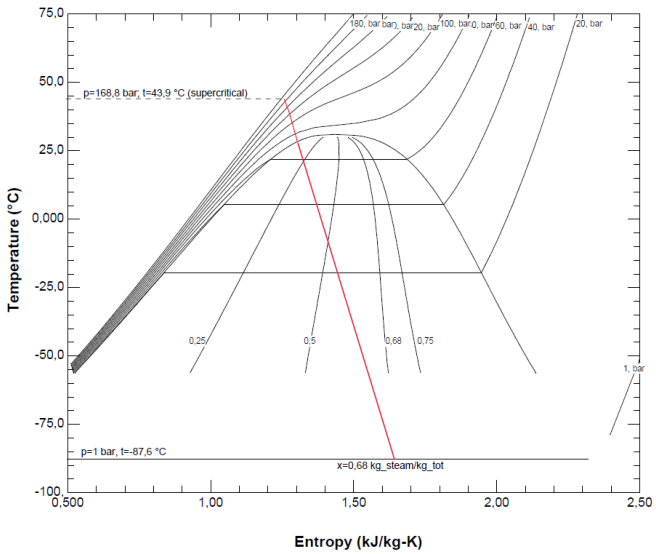

Figure 15: Throttling process after shaft-seal-failure scenario

As a result of the simulation, the short-term pressure increase in the oil tank due to a failure of the shaft-sealing system was calculated to be in the range of 100 mbar and therefore considered to be non-critical. After all these extensive tests, the loop was accepted for operation by TÜV Rheinland [7].

The start-up of the loop was a further challenge. Initial starting conditions were determined at 30 bar supplied by the CO_2 reservoir. A minimum starting temperature of 5 °C is required to avoid compressor operation in the two-phase region. This requirement also applies to the complete start-up sequence. After starting the machine, the compressor suction pressure was increased stepwise by filling the loop via an external high-pressure piston compressor while the temperature was controlled by cooling water. The duration needed for the pressurization was about four hours. The specific steps are shown in the Ts-diagram in Figure 16.

Thus, the nominal operating conditions on the compressor suction side (80 bar, 28 °C) are reached by following the path in the Ts-diagram around the dome, starting from gaseous to supercritical and finally to liquid state by avoiding the two-phase region. Figure 16 also shows the test-loop operating cycle (compression, valve expansion, and re-cooling).

DOI: 10.17185/duepublico/77319

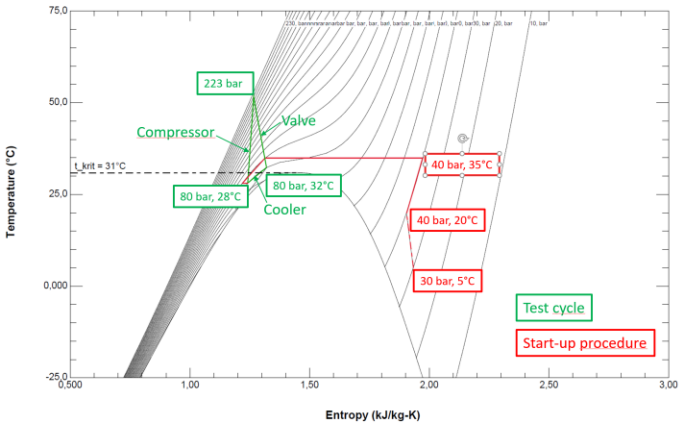

Figure 16: Ts-diagram of test-loop and start-up procedure

During the last step of the start-up sequence, it was found that accurate adjustment of the nominal operating point at the compressor inlet (80 bar, 28 °C) was a challenge due to the strong dependance of the pressure ratio and the density on the inlet temperature (see Figure 3).

However, after stable inlet operating conditions were reached, the subsequent performance test was carried out over a period of three hours without any incidents. Neither increased vibration levels were observed nor axial thrust issues during the test, which were previously considered as crucial items.

After the test, the machine was completely dismantled, and no indication of excessive wear was found on any of the main components, such as the impeller or the shaft seal system.

RESULTS

Besides demonstrating the fundamental compression process, the test objective was to compare theoretical design figures and the results from the CFD analysis with measurement data. Therefore, the measurement campaign included compressor operation at nominal inlet conditions from choke to near surge by setting the recycle valve.

Figure 17 shows the compressor performance curves comparing test data with CFD results. Additionally, the theoretical design point (DP) is added to the maps.

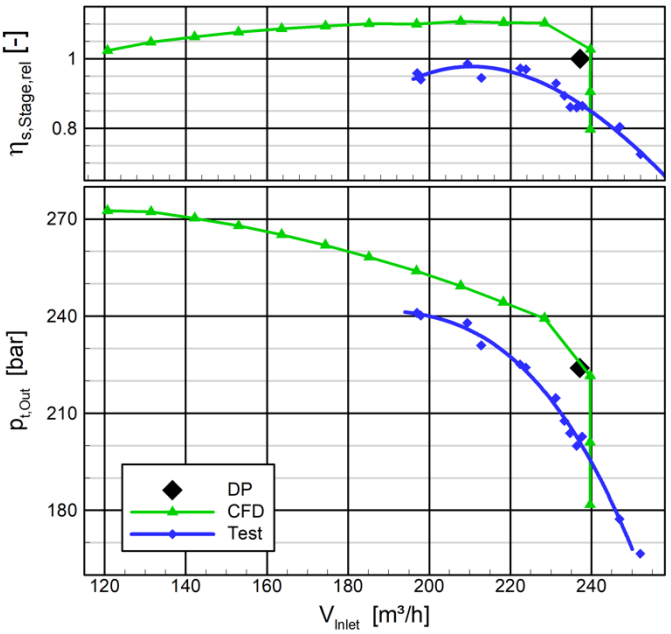

Figure 17: Total outlet pressure and relative isentropic efficiency vs inlet volume flow

A comparison of the measured and calculated pressure curves in Figure 17 shows a shift towards slightly lower pressure values for the test data, whereas the curve shape including rise to surge shows good agreement. This also applies to the prediction of the choke limit, just with a steeper decrease of the CFD curve.

Due to the maximum allowable working pressure in the loop of 242 bar, which was controlled by the safety relief valve, the measured curves are cut towards low volume flow. Therefore, the surge line was not reached experimentally, whereas the CFD calculation continues up to surge.

The points of maximum efficiency of both the measured and the calculated curves can be found at nearly the same flow. When compared to the theoretical design point, a shift towards lower flow values is observed. This indicates above all the influence of the impeller sealing gap, which was set to relatively high values during the test and in the CFD simulation, and led to increased recirculation mass flow rates, shifting the curves to lower flow rates.

One explanation for the deviation between the measured and predicted efficiency is the high measuring tolerances in the range of 1.8 %. The reason the measuring tolerances are high is because the impeller size is small and the temperature probes are protected by sleeves. Due to testing the machine at real operating conditions, there was no need to convert the test data except for the calculation of the isentropic head using the NIST REFPROP database.

In contrast, notable uncertainties of the CFD model have to be considered [8], which are basically higher than for standard

DOI: 10.17185/duepublico/77319

applications, such as high-pressure gradients within the impeller and diffuser (high pressure on small spatial dimensions).

Uncertainties arise from geometry model simplifications, such as not taking into account the back cavity and leakage through shaft seal (approx. 1%), possible deviations in all roughness assumptions (1-2%), as well as idealized blade geometry neglecting fillet radii, grooves and milling joints, which have a higher influence here due to the very low stage size (see Table 4).

Additional uncertainties are based on the mesh: discretization errors and the wall function approach (0.5 % each). Further impact comes from the possible model errors on both thermodynamics (interpolation table of real gas properties) and turbulence (underestimation of the turbulence on coarser grid accounts for 0.5-1 %).

Summing up the influencing factors on both experimental and CFD side, however, it can be concluded that the CFD model is able to predict the real machine behavior sufficiently.

SUMMARY AND CONCLUSION

In this paper, the design and the test-setup of a supercritical CO_2 compander were presented followed by the comparison of the compressor performance test results with a CFD analysis. While the machine delivered to the client is applied in a Brayton cycle to recover waste heat from a gas engine, a second identical unit was built for testing the compressor operating at the inlet slightly above the critical pressure but in the liquid phase of the CO_2. During the compression process, a sudden phase change of the CO_2 from the liquid to the supercritical state occurs, which is an innovation in the market. At these operating conditions, the compressor input work for compression is minimized, leading to the highest thermal efficiency of the cycle.

Therefore, the test was carried out with CO_2 at original operating conditions, which was a challenge for several reasons. For operating the compressor at the nominal suction conditions (80 bar, 28 °C), the start-up sequence included a stepwise pressurization of the loop following the path in the Ts-diagram around the dome by avoiding the two-phase region. Due to the excessive pressure and the hazardous working fluid, extensive safety measures were taken in advance, including a HAZOP meeting with TÜV Rheinland to determine the residual risks. As a result, the test-setup was accepted for operation.

During the test, a smooth operation at nominal operating conditions of the compressor could be demonstrated. The test data showed a slight shift of the pressure and efficiency curves towards lower flow and pressure, and lower efficiency values when compared to the CFD results but with good agreement concerning the curve shape, rise to surge, and choke limit.

Finally, both, the test data and the CFD results provide a valuable database for future sCO_2 machine designs.

NOMENCLATURE

η_{th}	Thermal cycle efficiency	(%)
P	Power	(kW)
$\dot{Q}$	Heat Flow	(kW)
h	Enthalpy	(kJ/kg)
p	Pressure	(Pa)
T	Temperature	(K)
s	Entropy	(kJ/kgK)
TÜV	Technischer Überwachungsverein	
GGI	General Grid Interface	
DP	Design Point	
Cv	Valve flow coefficient	(USPGM or m³/h)

REFERENCES

[1] Crespi, F., Gavagnin, G., Sánchez, D. and Martínez, G.S., 2017. *"Supercritical carbon dioxide cycles for power generation: A review"*. Applied Energy, 195, pp.152-183

[2] Lariviere B., Macadam S., McDowell S., Lesemann M., Marion J., 2021, *"sCO2 Power Cycle Development and STEP Demo Pilot Project"*, The 4th European sCO2 Conference for Energy Systems, Prague

[3] Vesely L., Prabu T., Gopinathan S., Otakar F., Subbaraman G. Kapat J., 2021, *"Greening a Cement Plant using sCO2 Power Cycle"*, The 4th European sCO2 Conference for Energy Systems, Prague

[4] Schuster S., Hacks A., Brillert D., 2022, *"Lessons from Testing the sCO2-HeRo turbo-compressor-system"*, 7th International Supercritical CO2 Power Cycles Symposium, San Antonio, Texas

[5] ANSYS CFX User Guide

[6] Honeywell UniSim Design User Guide

[7] TÜV Rheinland, Risikoorientierte Gefahrenanalyse ROGA Test Unit scCO2, 2020

[8] Toni L., Bellobuono E.F., Valente R., Romei A., et al, 2022, "Computational and Experimental Assessment of a MW-Scale Supercritical CO_2 Compressor Operating in Multiple Near-Critical Conditions", *Journal of Engineering for Gas Turbines and Power* Vol 144 (Issue 10), pp. 144-153

DOI: 10.17185/duepublico/77319

DOI: 10.17185/duepublico/77319
URN: urn:nbn:de:hbz:465-20230427-143506-8